Paintings by Turner and Monet Depict Trends in 19th Century Air Pollution

Anna Lea Albright[1*] and Peter Huybers[2]

[1*]Laboratoire de Météorologique Dynamique, CNRS, IPSL, rue Lhomond, 75005, Paris, France.
[2]Department of Earth and Planetary Sciences, Harvard University, Oxford Street, Cambridge, MA, 02138, United States.

*To whom correspondence should be addressed: anna-lea.albright@lmd.ipsl.fr;
This paper is a non-peer reviewed preprint submitted to EarthArXiv.

Abstract

Individual paintings by artists including Vincent van Gogh and Edvard Munch have been shown to depict specific atmospheric phenomena (1–6), raising the question whether longer-term environmental change influences stylistic trends in painting. Anthropogenic aerosol emissions increased to unprecedented levels during the 19th century as a consequence of the Industrial Revolution, particularly in Western European cities (7), leading to an optical environment having less contrast and more intensity (8–10). Here we show that trends from more figurative to impressionistic representations in J.M.W. Turner and Claude Monet's paintings in London and Paris over the 19th century accurately render physical changes in their local optical environment. In particular, we demonstrate that changes in local sulfur dioxide emissions are a highly statistically-significant explanatory variable for trends in the contrast and intensity of Turner, Monet, and others' works, including after controlling for time trends and subject matter. Industrialization altered the environmental context in which painting occurred, and our results indicate that Impressionism contains elements of polluted realism.

Some works of art, even those that do not appear 'realistic', appear to faithfully record particular natural phenomena. Edvard Munch's *The Scream* (1893), for example, is argued to depict nacreous clouds (6). Vincent van Gogh's *Moonrise* (1889) is dated to precisely 9:08 p.m. local time on July 13, 1889 using topographic observations, lunar tables, and letters (2). Nine of Claude Monet's paintings in his London series are also dated using solar geometry, with results confirmed by cross-referencing against Monet's letters (3). A survey of over 12,000 paintings, moreover, indicates that different schools reflect local meteorological conditions, such as paler blue skies in the British school than other contemporaneous European schools (1). Another important example of paintings depicting the natural environment comes from a set of studies of sunset coloration over time relative to volcanic eruptions that injected aerosols into the stratosphere (4, 5). Sunsets seen through an aerosol-laden stratosphere appear redder because of greater scattering in the limb of Earth's atmosphere (11). Across schools of painting, the red-to-green ratios in sunset paintings from 1500–1900 are correlated with independent proxies of stratospheric aerosol content (4, 5), though difficulty constraining the aerosol size distribution and solar zenith angle introduces uncertainties to this methodology (12).

Here we seek to ascertain whether there is a relationship between changes in atmospheric conditions associated with industrialization and changes in painting style — primarily that of the British artist Joseph Mallord William Turner (1775–1851) and French artist Claude Monet (1840–1926). We focus on Turner and Monet because they prolifically painted landscapes and cityscapes, often with repeated motifs. Furthermore, Turner and Monet's works span the Industrial Revolutions starting in Great Britain in the late 18th century, a time of unprecedented growth in air pollution (10, 13, 14). Over the course of their careers, Turner and Monet's painting styles change from sharper to hazier contours and towards a whiter palette, a progression that is typically characterized as moving from a more figurative to impressionistic style. We explore the hypothesis that increasingly impressionistic paintings by Turner, Monet, and several other artists represent, at least in part, physical changes in atmospheric optical conditions.

1 Optical implications of increasing aerosol concentrations

As illustrated in Fig. 1, aerosols absorb and scatter radiation both into and out of a line of sight. This scattering tends to decrease the contrast between otherwise distinct objects (e.g., 8, 9). Edges are used to quantify contrast because they often show the intensity of an object in the foreground relative to that of the background along nearly equal lines of sight. In order to objectively define contrast in a manner that adapts to the scale and perspective of an image, we use a wavelet technique. Wavelet analysis is selected over Fourier analysis because it allows for quantifying the local contrast in images (e.g., 15) and was previously used to estimate visibility in urban photographic images

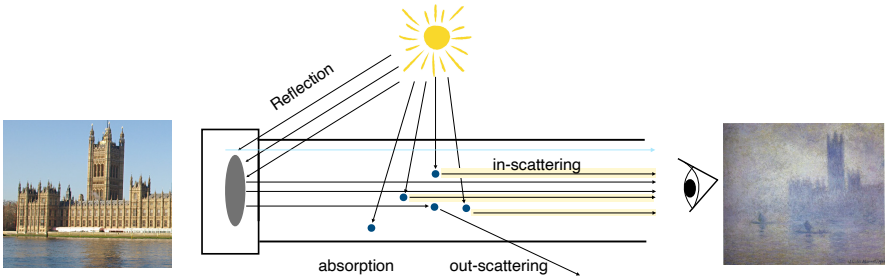

Fig. 1 Schematic illustrating key processes by which aerosols influence an object's contrast, intensity, and visibility. A theoretical object (denoted by the grey disk) reflecting light (black arrows) is visible because of its contrast with the background light (pale blue arrow). Aerosols (navy dots) in the air column (represented by the cylinder) scatter background light into the line of vision ('in-scattering', highlighted in light yellow), scatter object light out of the line of vision ('out-scattering'), and absorb light. These optical effects from aerosols lead a viewer to perceive an object as having less-distinct edges (less contrast) and a whiter tint (increased intensity), as idealized by the images on the left- and right-hand side and described in the Methods.

(16). We use a Haar wavelet whereby first differences of an image are taken at various scales (17), ranging from individual pixels to spanning the height or width of an image. An index of the contrast found in an image is obtained by computing the 95$^{\text{th}}$ percentile of the wavelet coefficients, w_{95}, normalizing by the median value, w_{50}, and taking the logarithm,

$$\text{contrast index} = \log(w_{95}/w_{50}). \tag{1}$$

Normalization accounts for different baseline edge strengths depending on lighting, scene, and image resolution, and the logarithm is suggested by the exponential dependence of contrast on the extinction coefficient (see Methods). Fig. S4 shows four example paintings illustrating that the largest gradients relate to distinct features, such as waves, a bridge, and the hull of ships.

1.1 Benchmarking with photographs

We first demonstrate our metric for contrast on pairs of photographs taken during clear and polluted conditions (Fig. S1). These photographic pairs involve less artistic interpretation and allow for benchmarking our technique using better-controlled image characteristics. Consistent with our expectations, every polluted photograph has a lower contrast index than its clear-sky counterpart (Fig. S1). The mean fractional reduction in the contrast index from clear-sky to polluted photographs is 19%. The same techniques used for photographs are next applied to evaluate trends in contrast in paintings, which are then evaluated in relation to aerosol emissions over time.

1.2 Quantifying historical air pollution

As a proxy for historic variations in anthropogenic aerosol concentrations, we use a gridded estimate of annual emissions of sulfur dioxide, SO_2 (18). The early Industrial Revolution was largely powered by coal (7, 10), and coal typically contains 1-5% sulfur by dry weight (19). From 1800–1850, the United Kingdom emitted nearly half of global SO_2 emissions, and the grid box corresponding to London, known as the 'Big Smoke' (10, 13, 14), accounts for approximately 10% of all United Kingdom SO_2 emissions (Fig. 2), despite accounting for only 1.0% of the area. Fig. S8 presents qualitative evidence for the optical effects associated with historical London air pollution captured by sketches and photographs.

SO_2 emissions are only a proxy for changes in atmospheric environment on account of aerosol concentration and size distribution at any particular time depending upon factors including co-emissions and local meteorology (e.g., 20, 21). Detrended British SO_2 emissions from 1800–1850, spanning Turner's artistic production, correlate with detrended black carbon (r=0.96) and organic carbon emissions (r=0.95), indicating that variability in SO_2 also generally tracks variability in other aerosol emissions and, thus, total aerosol concentrations. Later in the 19th century, however, the estimated emissions of black carbon and organic carbon per unit coal in England begin to decline (22). In London, in particular, political efforts to reduce industrial pollution (e.g., 10), shifts in cooking and heating sources from coal to gas (e.g., 7), and a more distributed urban landscape (e.g., 13) and expanded railway network also likely contribute to decreasing peak aerosol concentrations (e.g., 7, 14). We thus expect the magnitude of aerosol concentration associated with a given SO_2 emission rate to decrease over the course of the 19th century.

2 Trends in contrast in paintings by Turner, Monet, and others

We examine the contrast of 60 oil paintings by Turner spanning 1796–1850 and 38 paintings by Monet spanning 1864–1901. Across Turner's works (catalogued in Fig. S2) a progression is visually apparent from sharp to hazier contours, more saturated to pastel-like coloration, and figurative to impressionistic representation. A similar progression is evident across Monet's works (Fig. S3), with the additional factor that Monet's paintings are from two distinct locations. The first 18 of Monet's paintings, dating from 1864–1872, depict scenes in or near Paris, and all but one were painted before Monet's first visit to London from 1870–1871. The latter 20 paintings are from Monet's 1899–1901 visits to London, where he created serialized views of the House of Parliament, Waterloo Bridge, and Charing Cross Bridge.

A mixed effects model is used to evaluate whether local SO_2 emissions contribute to variations in contrast across our collection of Turner and Monet paintings. In our baseline formulation we specify fixed effects that capture

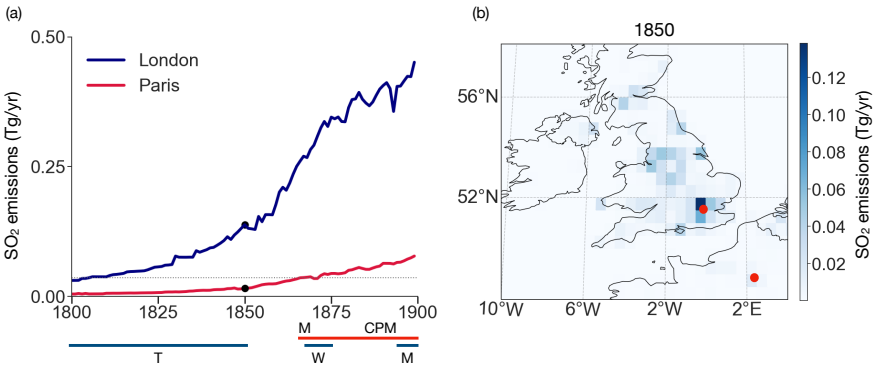

Fig. 2 19th century sulfur dioxide (SO_2) emissions in London and Paris. (a) Time series of emissions (18) in the grid boxes encompassing London (blue) and Paris (red). Years of paintings by Turner (T), Monet (M), Whistler (W), and Caillebotte, Pissarro, and Morisot (CPM) are indicated by horizontal lines for London (blue) and Paris (red). Emissions during Monet's early paintings correspond to those of Turner's early paintings (dotted black line represents mean Parisian emissions from 1864–1872). (b) A geographic distribution of SO_2 emissions in 1850, highlighting how emissions are concentrated in London (red point in England) and that emissions in Paris (red point in France around 2°E) trail those in London.

variations in contrast according to SO_2 emissions, year, and subject matter categories. We also allow for an interaction between year and SO_2 to account for co-emissions involved in producing atmospheric haze proportionately declining over time (22). Finally, the 98 paintings in our collections are partitioned into three categories, with 20 clear-sky, 46 cloudy, and 32 dawn or dusk paintings (see Methods).

Our baseline model explains 61% of the variance in the contrast index (Fig. 3, Table S1). As expected, paintings depicting dawn or dusk conditions or cloudy conditions have a lower contrast index ($p < 0.01$) relative to clear-sky conditions. Moreover, the model shows a significant reduction in contrast in response to increases in SO_2 emissions ($p < 0.01$), whereas the trend across years is indistinguishable from zero. The interaction effect is also significant ($p < 0.01$) and is consistent with the emissions of SO_2 later in time giving less change in the contrast index.

Six other model specifications are also explored that indicate that the significance of the SO_2 contribution is robust to excluding the year term or admitting for quadratic contributions from SO_2, year, or both (Table S1). Our baseline formulation is selected from among these models because it balances simplicity against the major features that we are concerned with capturing. Bayesian Information Criteria (BIC) offers a useful metric for this balance, where lower BICs indicate a more apt model. Our baseline specification gives among the

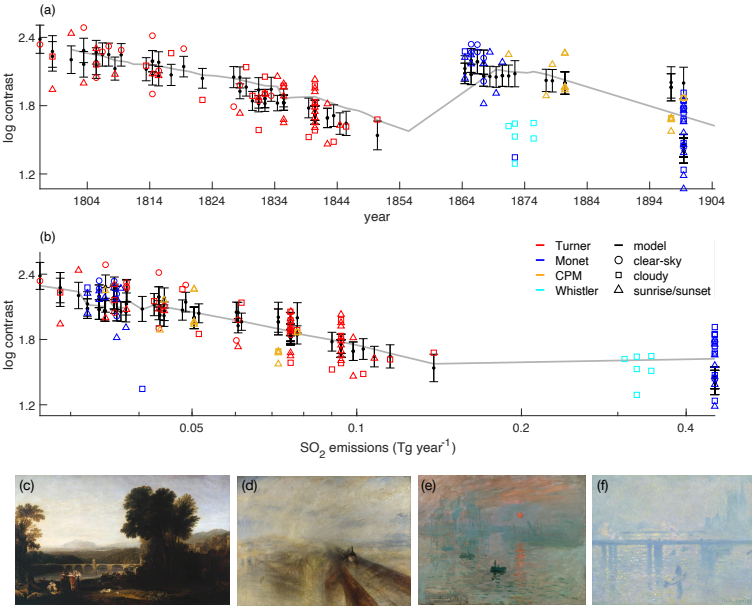

Fig. 3 Trends in the contrast index for different subject matter in the 60 Turner paintings (red) and 38 Monet paintings (blue) versus (a) year or (b) SO_2 emissions local to London or Paris. Also shown are six Whistler *Nocturnes* paintings (cyan), and seven paintings by Caillebotte, four by Pissarro, and one by Morisot (gold). Painting are categorized according to depicting conditions that are predominantly clear-sky (circle), cloudy (square), and dawn or dusk (triangle). Model predictions (black horizontal lines) are shown along with their 5–95% uncertainty (black vertical bars). Trends (gray lines) are illustrated by allowing year and SO_2 to vary but withholding categorical fixed effect. Monet's London paintings are plotted using 1899 London emissions because paintings were begun in the winter of 1899–1900, although exhibited in the following years, up until 1904. SO_2 is plotted on a logarithmic scale. Also shown are four representative paintings: (c) Turner's *Apullia in Search of Appullus* (1814), (d) Turner's *Rain, Steam, and Speed* (1844), (e) Monet's *Impression, Sunrise* (1872), and (f) Monet's *Charing Cross Bridge* (1899).

lowest BICs, though admitting for nonlinear dependencies on year and SO_2 gives comparable values. The highest BIC values result from excluding SO_2.

The primary reason that SO_2, as opposed to year, is inferred to control contrast relates to the fact that Paris and London have distinct SO_2 emission histories (Fig. 2). The magnitude of SO_2 emissions in London near the beginning of Turner's career in 1796 are similar to the magnitude of the emissions near the beginning of Monet's career in Paris in 1864. Monet's early paintings in Paris have higher contrast than most of Turner's works subsequent to the 1820s, despite coming later, such that no simple time trend can be fit across these collections (Fig. 3a). If examined in the context of SO_2 emissions,

however, the contrast of Monet's early works overlap with those of Turner's, and the low contrast of Monet's later works accord with the high emissions in London at the end of the 19th century (Fig. 3b).

Monet and Turner are among the most prolific and iconic artists whose work spans the industrial era, but paintings by other artists that depict cityscapes and atmospheric phenomena also align with our proposed model. Specifically, our model predicts the contrast found in seven paintings by Gustave Caillebotte (1848–1894), four paintings by Camille Pissarro (1830–1903), and one painting by Berthe Morisot (1841–1895) of Paris on the basis of year, local SO_2 emissions, and subject matter (Fig. 3). The contrast indices calculated for six *Nocturnes* paintings by Whistler in London between 1871–1875 are also predicted by our model. Note that Whistler's paintings in less-polluted environments — for example, *The Coast of Brittany* (1861) or *The Blue Wave Biarritz* (1862) — are associated with substantially greater contrast indices of 2.4 and 2.2, respectively. Refitting the linear mixed effects model to our expanded dataset of 116 works leads to conclusions that are consistent with our more limited analysis of only works by Turner and Monet (Fig. 3), but with the year trend now only appearing significant in the case where SO_2 is entirely excluded (Table S1).

3 Trends in intensity

As a complementary approach, it is also possible to analyse the intensity of images across our collection of works. Aerosols scatter visible light of all wavelengths into the line of sight (e.g., 23) (see Fig. 1), leading to a whiter tint and increased light intensity during daytime (e.g., 9). We examine the relationship between intensity and SO_2 emissions using the same mixed effects methodology used for contrast and find a significant effect ($p<0.01$) of SO_2 emissions increasing intensity in our baseline approach (Supplemental Table S2, Fig. S5). Of the 12 other specifications including SO_2, 9 show significant effects ($p<0.05$), including all those conditioned on the larger set of artists. Also similar to the contrast results, for the paired photographic analysis (Fig. S1), polluted photos have a uniformly increased intensity index, averaging 39% greater. The interpretation of intensity trends is complicated, however, in that variations in image intensity may result from accumulation of residue, fading of pigments, or photographic techniques (24), in addition to optical effects created by aerosols, such that we consider intensity secondary to contrast for purposes of indicating optical effects.

Visibility can be inferred from intensity using an empirical relationship (see Methods). Before 1830, visibility in clear-sky and cloudy Turner paintings averaged 25 km, whereas it decreased to an average of 10 km after 1830. For early Monet paintings, visibility averages 24 km, and for Monet's daytime paintings in London, visibility averages 5.6 km (Fig. S6). In comparison, (25) estimated visibility using the furthest clearly visible feature in 35 of Monet's Charing Cross Bridge paintings and found a mean of 1.1 km. They note that

the *London Fog Inquiry* describes visibility in the winter of 1901–1902 as never being more than approximately 2 km. Differences could arise due to uncertainties in both methodologies – the imprecision of estimating visibility by eye for (25), and, in addition to the aforementioned issues with interpreting intensity, there are various limiting assumptions in our model of visibility (see Methods).

4 Style versus nature

It is clear that industrialization changed the environmental context in which painting occurred. Indeed, 19th art critic John Ruskin wrote about Turner's work that, "had the weather when I was young been such as it is now, no book such as 'Modern Painters' ever would or could have been written" (26). A primary question, however, is the degree to which trends towards decreased contrast and increased intensity represent physical, optical changes associated with a polluted atmosphere, as opposed to exerting an indirect influence on artistic style. Beyond the statistical results discussed earlier, two further considerations suggest that environmental trends are rendered in the works we consider.

First, and rather obviously, the environment that these artists depict was, in fact, subject to large trends in atmospheric pollution (18). Turner was born in the age of sail and died in an age of coal and steam (27). It is important to recognize, however, that not all artists depict a changed atmospheric environment. For example, John Constable (1776–1837) created works that show neither the diminished contrast nor increased intensity expected from London's aerosol-laden atmosphere. It may be that certain artists chose times and locations where the effects of pollution were minimal. Indeed, whereas Constable remarked that Turner seems to paint with "tinted steam" (28), he himself was known to leave London for less-polluted Hampstead Heath or the Lake District (29).

The second consideration is more speculative as it relates to motivation and approach. Turner sought to represent technological and resulting environmental change (27), especially as it relates to atmospheric effects on light. In *The Fighting Temeraire* (1839), perhaps Turner's most iconic work, a steam-powered tugboat pulls the HMS Temeraire, a military sailing ship made famous by the 1805 Battle of Trafalgar, to land to be broken up for scrap against a backdrop of a fiery setting sun, illustrating the transition from the age of sail to steam. Similarly, *Rain, Steam, and Speed* (1844) depicts a train racing through the British countryside, contrasted with symbols of the past age, such as a row boat gliding over the water, a hare, the fastest natural animal in Britain, running from the oncoming train, and a farmer plowing without mechanized equipment, all almost lost in mist.

That Turner should be among the first to depict changes in how light transmits through the atmosphere might be traced to a general increase in the scientific understanding of light and the sky that occurred concurrently in England with Turner's career (30). In 1801, astronomer William Herschel gave

a lecture, "The Nature of the sun" (31), which is thought to have influenced how Turner paints the brightness and texture of the sun (27) (Fig. S7a). In 1803, meteorologist Luke Howard published *On the Modification of Clouds* that introduced the cloud classification of cumulus, stratus, and cirrus (32), which was featured in art manuals and even inspired a poem by Johann Wolfgang von Goethe (1749–1832) (29). Fig. S7b shows cloud studies by Luke Howard, and, roughly synchronously, by Turner.

An important analogue case is Turner's documentation of the 1815 Tambora volcanic eruption. Turner depicts changes in sunset coloration that accord with the expected effects of volcanism (4, 5). Turner also produced a sketchbook of 65 watercolors of sunsets in the three years following the Tambora eruption that captures the waxing and waning of the atmospheric reddening associated with stratospheric sulphate injection (Fig. S7c). The fact that the course of events that Turner documents is consistent with the expected timescale associated with stratospheric sulphate migration and deposition following a volcanic eruption (e.g., one to three years, 33) is further evidence for Turner providing a faithful depiction of atmospheric light phenomena.

If it is accepted that the optical consequences of increased atmospheric pollution are depicted in the body of work by Turner, Monet, and others, a question arises whether it is possible to calibrate the depicted trends for making inferences regarding atmospheric composition. There are no direct, empirical measurements of urban air pollution during early industrialization (e.g., 34). The mechanistic process associated with recording environmental conditions using paint and canvas is, however, of similar complexity to any natural proxy of the environment, such as tree rings or ice cores. Aesthetic considerations then add additional layers of interpretation. One issue is that Monet and Whistler appear to have been influenced by Turner's style (35). Turner's *Rain, Steam, and Speed*, for example, was one of the few paintings by other artists that Monet directly referred to in his correspondence (36).

A related issue in considering whether atmospheric composition can be inferred is that the scenes sampled in these works are not chosen at random. Monet, for example, writes, "What I like most of all in London is the fog" (10) and, "when I got up I was terrified to see that there was no fog, not even a wisp of mist: I was prostrate, and could just see all my paintings done for, but gradually the fires were lit and the smoke and haze came back" (37). Note that the word 'smog' for smoke and fog was not coined until 1905 (e.g., 10). The impressionistic movement may have led some artists to focus upon atmospheric effects that highlight the influence of aerosol emissions upon the atmosphere, in which case trends in painting characteristics may amplify upon actual environmental trends.

We also mention a hypothesis that ascribes trends in Turner's works towards haziness to increasingly faulty vision (38). There is no direct evidence, however, that Turner had poor eyesight that would be responsible for increased haziness of his paintings and, moreover, Turner continued to paint details in the foreground (39). Similarly, (39) demonstrates that Monet was not myopic

and that he only suffered from cataracts decades after he began painting more impressionistic works. Conversely, it appears that loss of visual acuity associated with the development of cataracts led Edgar Degas (1834–1917) to paint with a different palette and in less detail (40).

5 Conclusions

Our basic premise is that Impressionism — as developed in the works of Turner, Monet, and others — contains elements of polluted realism. Over the 19th century, the atmospheric reality in London and Paris changed. Turner, Monet, and others document these changes in paint, yielding proxy evidence for historical trends in atmospheric pollution before instrumental measurements of air pollution become available. A mixed effects model including both temporal and environmental trends can explain 61% of the variance in a contrast index and gives a significant dependence on SO_2 emissions for each statistical model specification, including after controlling for year and subject matter. These results indicate that a combination of trends in style and atmospheric pollution contribute to trends in the contrast of Turner and Monet's paintings. The magnitude of the changes in paintings are plausible relative to changes between contemporary pairs of clear-sky and polluted photographs. Estimates of intensity generally correspond with those of contrast, but are noisier and less significant. Visibility inferred from the London works by Monet are also in keeping with historical records of visibility.

Issues associated with scene selection and the atmospheric chemistry of smog would need to be controlled for before quantitative inferences of mean atmospheric conditions are possible from this sample of paintings. We are, moreover, not able to resolve seasonality in atmospheric conditions, principally because few paintings depict winter conditions. Nevertheless, the evidence that we present for Turner, Monet, and others depicting physical atmospheric conditions suggests new opportunities for appreciating and interpreting their artwork. Our view is that impressionistic paintings recording natural phenomena — as opposed to being imagined, amalgamated, or abstracted — does not diminish their significance; rather, it highlights the connection between environment and art. Furthermore, our results suggest that environmental change provided a creative impulse whereby the importance of lines and edges was diminished in favor of demarcating objects using color fields.

A historical connection between aerosols and painting style also supports insights into societal responses to contemporary human-caused environmental changes. The relevance of such comparisons is highlighted by the fact that megacities such as Beijing, New Delhi, and Mexico City have levels of air pollution similar to those of 19th London (e.g., 41). Furthermore, if stratospheric solar radiation management were used to mitigate climate risks (e.g., 42, 43), it would increase the intensity, or whiteness, of the sky and globally diminish the contrast of objects viewed against this background. Our findings suggest

that modern changes to atmospheric properties can also be expected to both literally and figuratively change how we see the world.

References

[1] Neuberger, H.: Climate in art. Weather **25**(2), 46–56 (1970)

[2] Olson, D.W., Doescher, R.L., Olson, M.S.: Dating van Gogh's "Moonrise" (2003)

[3] Baker, J., Thornes, J.E.: Solar position within Monet's Houses of Parliament. Proceedings of the Royal Society A: Mathematical, Physical and Engineering Sciences **462**(2076), 3775–3788 (2006)

[4] Zerefos, C.S., Gerogiannis, V., Balis, D., Zerefos, S., Kazantzidis, A.: Atmospheric effects of volcanic eruptions as seen by famous artists and depicted in their paintings. Atmospheric Chemistry and Physics **7**(15), 4027–4042 (2007)

[5] Zerefos, C., Tetsis, P., Kazantzidis, A., Amiridis, V., Zerefos, S., Luterbacher, J., Eleftheratos, K., Gerasopoulos, E., Kazadzis, S., Papayannis, A.: Further evidence of important environmental information content in red-to-green ratios as depicted in paintings by great masters. Atmospheric Chemistry and Physics **14**(6), 2987–3015 (2014)

[6] Fikke, S.M., Kristjánsson, J.E., Nordli, Ø.: Screaming clouds. Weather **72**(5), 115–121 (2017)

[7] Fouquet, R.: Long run trends in energy-related external costs. Ecological Economics **70**(12), 2380–2389 (2011)

[8] Horvath, H.: On the applicability of the Koschmieder visibility formula. Atmospheric Environment (1967) **5**(3), 177–184 (1971)

[9] Kim, K.W., Kim, Y.J.: Perceived visibility measurement using the hsi color difference method. Journal of the Korean Physical Society **46**(5), 1243 (2005)

[10] Corton, C.L.: London fog. Harvard University Press (2015)

[11] Meinel, A., Meinel, M.: Sunsets, twilights, and evening skies. Cambridge University Press (1991)

[12] von Savigny, C., Lange, A., Hemkendreis, A., Hoffmann, C., Rozanov, A.: Is it possible to estimate aerosol optical depth from historic colour paintings? Climate of the Past Discussions, 1–15 (2022)

[13] Brimblecombe, P.: London air pollution, 1500–1900. Atmospheric Environment (1967) **11**(12), 1157–1162 (1977)

[14] Brimblecombe, P.: The Big Smoke: A history of air pollution in London since medieval times. Routledge (2012)

[15] Strang, G., Nguyen, T.: Wavelets and filter banks. SIAM Journal on Applied Mathematics (1996)

[16] Luo, C.-H., Yuan, C.-S., Wen, C.-Y., Liaw, J.-J., Chiu, S.-H., *et al.*: Investigation of urban atmospheric visibility hsing haar wavelet transform. Aerosol and Air Quality Research **5**(1), 39–47 (2005)

[17] Haar, A.: Zur theorie der orthogonalen funktionensysteme. Georg-August-Universitat, Gottingen. (1909)

[18] Hoesly, R.M., Smith, S.J., Feng, L., Klimont, Z., Janssens-Maenhout, G., Pitkanen, T., Seibert, J.J., Vu, L., Andres, R.J., Bolt, R.M., *et al.*: Historical (1750–2014) anthropogenic emissions of reactive gases and aerosols from the community emissions data system (CEDS). Geoscientific Model Development **11**(1), 369–408 (2018)

[19] Calkins, W.H.: The chemical forms of sulfur in coal: a review. Fuel **73**(4), 475–484 (1994)

[20] He, H., Wang, Y., Ma, Q., Ma, J., Chu, B., Ji, D., Tang, G., Liu, C., Zhang, H., Hao, J.: Mineral dust and nox promote the conversion of so 2 to sulfate in heavy pollution days. Scientific reports **4**(1), 1–6 (2014)

[21] Zheng, B., Zhang, Q., Zhang, Y., He, K., Wang, K., Zheng, G., Duan, F., Ma, Y., Kimoto, T.: Heterogeneous chemistry: a mechanism missing in current models to explain secondary inorganic aerosol formation during the january 2013 haze episode in North China. Atmospheric Chemistry and Physics **15**(4), 2031–2049 (2015)

[22] Junker, C., Liousse, C.: A global emission inventory of carbonaceous aerosol from historic records of fossil fuel and biofuel consumption for the period 1860–1997. Atmospheric Chemistry and Physics **8**(5), 1195–1207 (2008)

[23] Boucher, O.: Atmospheric aerosols. Springer (2015)

[24] Martinez, K., Cupitt, J., Saunders, D., Pillay, R.: Ten years of art imaging research. Proceedings of the IEEE **90**(1), 28–41 (2002)

[25] Thornes, J.E., Metherell, G.: Monet's 'London series' and the cultural climate of London at the turn of the Twentieth century. Weather, climate,

culture, 141–60 (2003)

[26] Ruskin, J.: The art of England: Lectures given in Oxford. George Allen (1884)

[27] Hamilton, J.: Turner and the Scientists. Tate Gallery Publishing London (1998)

[28] Tate: Turner's Modern World. https://www.tate.org.uk/whats-on/tate-britain/exhibition/turners-modern-world Accessed 2011-21-07

[29] Hamblyn, R.: The invention of clouds: How an amateur meteorologist forged the language of the skies. Macmillan (2002)

[30] Reno, S.T.: Air: Clouds and Climate Change in the Nineteenth Century. Springer (2020)

[31] Herschel, W.: XIII. Observations tending to investigate the nature of the sun, in order to find the causes or symptoms of its variable emission of light and heat; with remarks on the use that may possibly be drawn from solar observations. Philosophical Transactions of the Royal Society of London (91), 265–318 (1801)

[32] Howard, L.: On the modification of clouds', Essay to the Askesian Society. Taylor, London (1803)

[33] Robock, A.: Volcanic eruptions and climate. Reviews of geophysics **38**(2), 191–219 (2000)

[34] Fowler, D., Brimblecombe, P., Burrows, J., Heal, M.R., Grennfelt, P., Stevenson, D.S., Jowett, A., Nemitz, E., Coyle, M., Liu, X., *et al.*: A chronology of global air quality. Philosophical Transactions of the Royal Society A **378**(2183), 20190314 (2020)

[35] Britain, T.: Turner, Whistler, Monet, Press Release. https://www.tate.org.uk/press/press-releases/turner-whistler-monet (2005)

[36] Shanes, E.: Impressionist London. Abbeville Press London (1994)

[37] Patin, S.: Claude Monet in Great Britain. Hazan (1994)

[38] Liebreich, R.: Turner and Mulready: The Effect of Certain Faults of Vision on Painting with Especial Reference to Their Works; The Real and Ideal in Portraiture; The Deterioration of Oil Paintings. J. & A. Churchill (1888)

[39] Marmor, M.: Vision, eye disease, and art: 2015 Keeler Lecture. Eye **30**(2), 287–303 (2016)

[40] Marmor, M.F.: Ophthalmology and art: simulation of Monet's cataracts and Degas' retinal disease. Archives of ophthalmology **124**(12), 1764–1769 (2006)

[41] Mage, D., Ozolins, G., Peterson, P., Webster, A., Orthofer, R., Vandeweerd, V., Gwynne, M.: Urban air pollution in megacities of the world. Atmospheric environment **30**(5), 681–686 (1996)

[42] Keith, D.W.: Geoengineering the climate: History and prospect. Annual review of energy and the environment **25**(1), 245–284 (2000)

[43] Crutzen, P.J.: Albedo enhancement by stratospheric sulfur injections: a contribution to resolve a policy dilemma? Climatic change **77**(3-4), 211 (2006)

Acknowledgments. We thank Peter Brimblecombe, Fabienne Chevallier, Kerry Emanuel, Roger Fouquet, Bernhard Mayer, and Robin Wordsworth for helpful feedback on an earlier version of this manuscript. ALA and PJH performed the analysis and wrote the manuscript. The authors declare no competing interests. Painting, photograph, and SO_2 data are available at https://doi.org/10.7910/DVN/YQOLZW. The code to generate the plots and perform the relevant analyses will be made available with a DOI.

Supplementary Materials. These supplementary materials include:
Methods
Tables S1 to S2
Figs. S1 to S8

Supplemental Materials for Paintings by Turner and Monet Depict Trends in 19th Century Air Pollution

Anna Lea Albright[1*] and Peter Huybers[2]

[1*]Laboratoire de Météorologique Dynamique, CNRS, IPSL, rue Lhomond, 75005, Paris, France.
[2]Department of Earth and Planetary Sciences, Harvard University, Oxford Street, Cambridge, MA, 02138, United States.

*To whom correspondence should be addressed:
anna-lea.albright@lmd.ipsl.fr;

Included in these supplemental materials are Methods, supplemental tables S1–S2, and supplemental figures Fig. S1–S8.

1 Methods

1.1 Theoretical expectations of contrast and visibility

As the distance, dx, between an observer and object increases, the intensity of light from the object, $I_o(x)$, increases as a result of diffuse background light scattered into the line of sight, $\sigma_b I_b(x)$, and decreases as a result of scattering and absorption along the line of sight, $\sigma_e I_o(x)$,

$$\frac{dI_o(x)}{dx} = \sigma_b I_b(x) - \sigma_e I_o(x). \tag{1}$$

When particles are present, dx is proportional to the number of suspended aerosol particles in the air column. The isotropic scattering coefficient, σ_b, represents the efficiency with which background light is scattered into the line of sight, and the extinction coefficient, σ_e, represents how much intensity is lost through absorption and scattering as a beam of light passes through a material. Both coefficients are in units of inverse meters.

Unlike for a finite object, background radiation is assumed to be independent of x, given homogeneous, isotropic background scattering, and therefore,

$$\frac{dI_b(x)}{dx} = \sigma_b I_b(x) - \sigma_e I_b(x) = 0. \tag{2}$$

It follows that σ_b equals σ_e.

Replacing σ_b with σ_e in Eq. (1), integrating intensity from 0 to I and distance from 0 to X, and taking the logarithm yields,

$$\frac{I_b(x) - I_o(x)}{I_b(x)} = \exp(-\sigma_e X) \tag{3}$$

The left-hand side of Eq. (3) is defined as the contrast, $C(x)$, or the relative difference between $I_b(x)$ and $I_o(x)$,

$$C(x) = \exp(-\sigma_e X). \tag{4}$$

A black object a distance $x = 0$, for instance, has $I_o(0) = 0$, by definition, yielding a contrast of one. Eq. (3) is a version of the Beer-Lambert law where contrast decreases exponentially with distance from an object, dx, or with particle concentration when particles are present. Assumed in this representation is that both the background and object intensities are seen along nearly the same lines of sight and that the background intensity is independent of direction (e.g., 1).

Taking the logarithm of Eq. (4) and rearranging yields,

$$X = \frac{-\ln(C(x))}{\sigma_e}. \tag{5}$$

Earlier studies assumed that a contrast threshold of $C(x) = 0.02$ was the perceptible limit, or farthest distance one can detect a dark object against a light background (2). We follow more-recent studies in using a contrast threshold of 0.05 (3, 4), yielding a highly-idealized estimate of visibility, X_{v}, as an inverse function of the extinction coefficient, σ_{e},

$$X_{\mathrm{v}} = \frac{3.0}{\sigma_{\mathrm{e}}}, \tag{6}$$

known as the Koschmieder equation (2).

1.2 Intensity and visibility

We quantify the amount of white light using the hue-saturation-intensity color model, where intensity ranges from black, with a value of zero, to white with a value of one (5). We consider the median-intensity across all image pixels, referred to as the intensity index. The image median is simple to define, though an analysis of only the sky or other common features could also be instructive.

It is possible to estimate σ_{e} from anomalies in intensity using an empirical function derived from photographic observations (6),

$$\sigma_{\mathrm{e}} = 3.4 \times 10^{-7} \exp\left(14.7(\bar{I} - \bar{I}_{95})\right) + 1.1 \times 10^{-4}. \tag{7}$$

$\bar{I}$ is the image-median intensity, which ranges from 0.1 to 0.8 across the images of paintings that we consider (Fig. S5) and between 0.3 to 0.9 among the urban photographs we consider (Fig. S1). Depending on the application of Eq. 7, $\bar{I}_{95}$ is the 95$^{\mathrm{th}}$ percentile of the clear-sky paintings in our collection, 0.65, or the 95$^{\mathrm{th}}$ percentile of clear-sky photographs in our collection, 0.75. Note that Eq. 7 is rewritten from (6) to be in units of inverse meters and to depend on intensity scaled between 0 and 1.

A less-idealized estimate of σ_{e} would be possible taking into account zenith angle of the sun, the position of the observer, and the direction of view, but such information is not readily available for most of the paintings we consider. The images we consider, moreover, are not digitized under identical conditions, which inevitably introduces noise to the samples.

Substituting Eq. (7) for σ_{e} into Eq. (6) gives an estimate of the visibility range associated with various paintings (Fig. S6). For early Turner works, our visibility ranges are broadly consistent with ranges of 20–30 km for contemporary clear-sky urban conditions (e.g., 7) and, for Turner's later works, as well as Monet's London paintings, visibility ranges are consistent with the 1–5 km range estimated for contemporary strong urban haze conditions (6). Visibility estimates below 5 km for late 19$^{\mathrm{th}}$ century London are in keeping with estimates for contemporary megacities during strong urban haze conditions, such as Delhi (e.g., 8) and Beijing (e.g., 9, 10).

Fractional changes in contrast and intensity indices are also calculated for comparison with photographs. This percent change is calculated only

for Turner paintings (e.g., by subject matter, such as predominantly clear-sky) by dividing these paintings into two groups and computing, $(I_{\text{late}} - I_{\text{early}})/I_{\text{early}} \times 100$, wherein paintings in each category are divided into two equally-sized groups for early and late. For photographs, the percent change is calculated between clear-sky and polluted photographs.

1.3 Wavelet analysis of contrast

Wavelet analysis is performed by convolving grayscale image matrices with a two-dimensional, multi-scale Haar wavelet using the Python package, *PyWavelets* and, specifically, the *wavedec2* function (11). The Haar wavelet consists of a hierarchy of square-wave-shaped functions,

$$\psi(t) = \begin{cases} 1 & 0 \le t < \frac{1}{2}, \\ -1 & \frac{1}{2} \le t < 1, \\ 0 & \text{otherwise}, \end{cases} \tag{8}$$

Graycale image matrices are calculated as a weighted sum of the corresponding red, green, and blue pixels, $\mathrm{X} = 0.2125\mathrm{R} + 0.7154\mathrm{G} + 0.0721\mathrm{B}$, though results are qualitatively similar for individual color channels.

High-pass, or, detailed coefficients, are interpreted because of interest in the representation of abrupt features. Seven scales are used for the Haar wavelets, although similar results are obtained using fewer scales. Coefficients can be computed in the horizontal, vertical, and diagonal direction, and we use horizontal coefficients that emphasize horizontal edges (e.g., 12).

An index of the contrast found in an image is computed as the 95$^{\text{th}}$-percentile of all high-pass horizontal coefficients divided by the median (see Eq. (**??**) in Sec. 1. Selection of the 95$^{\text{th}}$-percentile represents a balance between identifying among the sharpest features in an image and guarding against being overly sensitive to outliers. Using other high percentiles, however, such as the 90$^{\text{th}}$ or 99$^{\text{th}}$, gives similar results. Normalization by the median of the coefficients accounts for different baseline edge strengths depending on lighting, scene, and image resolution.

1.4 Mixed effects model formulation

Our baseline mixed effects model (e.g., 13) for the contrast index is formulated as,

$$\log \text{contrast} = \alpha_0 + \alpha_1 \text{year} + \alpha_2 \mathrm{SO}_2 + \alpha_3(\text{type}) + \alpha_4 \text{year}^* \mathrm{SO}_2 + \epsilon_c. \tag{9}$$

This model involves fixed effect terms for year, SO_2, the interaction between year and SO_2, and categorical effects associated with subject matter (type) according to clear-sky, cloudy, or dawn/dusk conditions. Allowing for random intercepts or slopes, such as for type, does not improve the fit as judged by either the Akaike or Bayesian Information Criteria, consistent with our prior

expectation of a non-zero contribution to contrast from each factor. The year is represented as the anomaly from the mean. The interaction term between year and SO_2 captures the weakening effect of a given amount of SO_2 to the total aerosol concentration (see Sec. 1.2). This interaction term is positive and offsets the negative contribution to contrast solely from SO_2, which over-predicts decreases in contrast when SO_2 is considered individually, without the interaction term.

This model formulation allows for examining how SO_2 emissions influences contrast across paintings after controlling for effects associated with temporal trends and selection of subject matter. Although year and SO_2 are correlated (R^2=0.47), the fact that London and Paris have different SO_2 time histories permits for distinguishing simple time trends from environmental trends.

Results for our primary specifications are given in supplemental Table S1 including only works by Turner (60) and Monet (38) on row 1 and for also including 6 works by Whistler, 7 by Caillebotte, 4 by Pissarro, and 1 by Morisot on row 7. Six alternative specification are also examined: omitting the interaction term between year and SO_2, omitting the interaction and SO_2 terms, omitting the interaction and year terms, omitting the interaction term but including a term for SO_2^2, omitting the interaction term but including year^2, and omitting the interaction term but including both year^2 and SO_2^2. Specifications 8–14 are equivalent to 1–7 but applied to the larger collection of 116 paintings.

Similarly, a linear model for the intensity index is formulated as,

$$\text{intensity} = \beta_0 + \beta_1 \text{year} + \beta_2 \text{SO}_2 + \beta_3(\text{type}) + \beta_4 \text{year*SO}_2 + \epsilon_i. \qquad (10)$$

Table S2 reports results for the baseline formulations for Turner and Monet paintings (row 1) and for all paintings (row 7), as well as six alternative specifications as for contrast (14 specifications total; seven for Turner and Monet paintings, and another seven the larger collection of paintings).

	R^2	BIC	year	SO_2	dawn	cloudy	year*SO_2
1.	0.61	-25.1	-0.46** (-0.69 -0.23)	-5.42** (-6.86 -3.99)	-0.09	-0.12*	0.09**
2.	0.43	6.6	-0.04 (-0.27 0.19)	-0.81** (-1.29 -0.34)	-0.21**	-0.23**	-
3.	0.36	13.1	-0.35** (-0.50 -0.20)	-	-0.27**	-0.24**	-
4.	0.43	2.2	-	-0.89** (-1.18 -0.59)	-0.22**	-0.23**	-
5.	0.61	-26.1	-0.14 (-0.34 0.05)	-8.19** (-10.40 -5.98)	-0.08	-0.11*	-
6.	0.57	-17.2	0.33** (0.09 0.56)	-2.32** (-2.98 -1.66)	-0.12	-0.14**	-
7.	0.61	-22.5	-0.36 (-0.84 0.12)	-10.44** (-15.47 -5.42)	-0.08	-0.11*	-
8.	0.60	-28.2	-0.52** (-0.73 -0.32)	-4.85** (-6.08 -3.61)	-0.10	-0.11*	0.09**
9.	0.45	4.7	-0.04 (-0.21 0.13)	-0.84** (-1.21 -0.46)	-0.22**	-0.21**	-
10.	0.36	17.8	-0.29** (-0.44 -0.15)	-	-0.28**	-0.21**	-
11.	0.45	0.1	-	-0.89** (-1.18 -0.61)	-0.22**	-0.22**	-
12.	0.63	-35.5	-0.12 (-0.27 0.03)	-8.62** (-10.72 -6.51)	-0.08	-0.10	-
13.	0.50	-1.3	0.08 (-0.10 0.26)	-1.27** (-1.72 -0.83)	-0.19**	-0.18**	-
14.	0.63	-31.3	-0.16 (-0.33 0.02)	-9.11** (-11.58 -6.64)	-0.07	-0.10	-

Table 1 Summary statistics for mixed effects models of log contrast. For each of 14 specifications we report variance explained by each model (R^2), the Bayesian Information Criteria (BIC), and the fixed effects coefficients for year (contrast index units per century), SO_2 (contrast index units per Tg SO_2 emitted per year), interaction between year and SO_2, and categorical offsets from a clear-sky baseline for paintings depicting dawn/dusk or cloudy conditions (contrast index units). The 95% confidence interval for fixed effects associated with year and SO_2 are reported parenthetically. Coefficients that differ from 0 at $p < 0.05$ are indicated by '*' and by $p < 0.01$ by '**'. The baseline specification, no. 1, is for the contrast index in the 98 Turner and Monet paintings to equal $\alpha_0 + \alpha_1 \text{year} + \alpha_2 SO_2 + \alpha_3(\text{type}) + +\alpha_4 \text{year*} SO_2 + \epsilon_c$, wherein $\alpha_3(\text{type})$ is expanded as $\alpha_{\text{dusk}} + \alpha_{\text{cloud}}$. Specification 2 omits the interaction term between year and SO_2; 3 omits the interaction and SO_2 terms; 4 omits the interaction and year terms; 5 omits the interaction term but includes a term for SO_2^2; 6 omits the interaction term but includes year^2; and 7 omits the interaction term but includes both year^2 and SO_2^2. Specifications 8–14 are equivalent to 1–7 but applied to a collection of 116 paintings that include works by Whistler, Caillebotte, Pissarro, and Morisot.

	R^2	BIC	year	SO_2	dawn	cloudy	year*SO_2
1.	0.37	-90.4	0.36** (0.20 0.53)	2.32** (1.29 3.35)	0.04	0.07	-0.04**
2.	0.23	-75.3	0.15* (0.00 0.31)	-0.01 (-0.32 0.31)	0.10*	0.13**	-
3.	0.23	-79.9	0.15** (0.06 0.25)	-	0.10*	0.13**	-
4.	0.19	-75.9	-	0.24* (0.04 0.44)	0.10*	0.14**	-
5.	0.36	-89.2	0.20** (0.06 0.34)	3.57** (1.97 5.17)	0.04	0.07	-
6.	0.38	-92.8	-0.06 (-0.22 0.10)	0.88** (0.43 1.33)	0.05	0.08*	-
7.	0.38	-88.2	-0.10 (-0.44 0.24)	0.46 (-3.14 4.05)	0.05	0.08*	-
8.	0.35	-103.6	0.38** (0.23 0.53)	2.09** (1.20 2.98)	0.04	0.07	-0.04**
9.	0.22	-88.0	0.13* (0.01 0.25)	0.04 (-0.22 0.29)	0.10*	0.12**	-
10.	0.22	-92.7	0.14** (0.05 0.23)	-	0.10*	0.12**	-
11.	0.19	-88.0	-	0.22* (0.02 0.42)	0.11*	0.14**	-
12.	0.35	-103.7	0.17** (0.06 0.28)	3.74** (2.17 5.31)	0.03	0.07	-
13.	0.30	-95.9	0.04 (-0.08 0.16)	0.36* (0.06 0.65)	0.08	0.10**	-
14.	0.35	-100.3	0.13 (-0.00 0.26)	3.17** (1.34 5.01)	0.04	0.07	-

Table 2 Summary statistics for mixed effects models of intensity. As for Table S1, but Whistler's *Nocturnes* paintings are excluded, as they depict dark, nighttime conditions that, by definition, have much lower intensity.

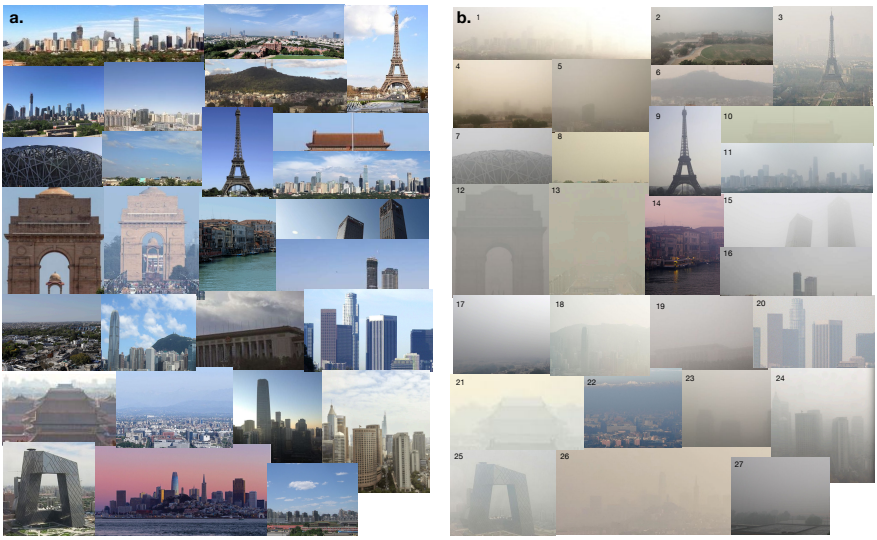

Fig. 1 27 pairs of contemporary clear-sky (a.) and polluted (b.) photographs that depict the same scene but differ in the level of pollution. (c) Log-contrast values for clear-sky (blue) and polluted (grey) photographs, and (d) image-median intensity values for clear-sky and polluted photographs.

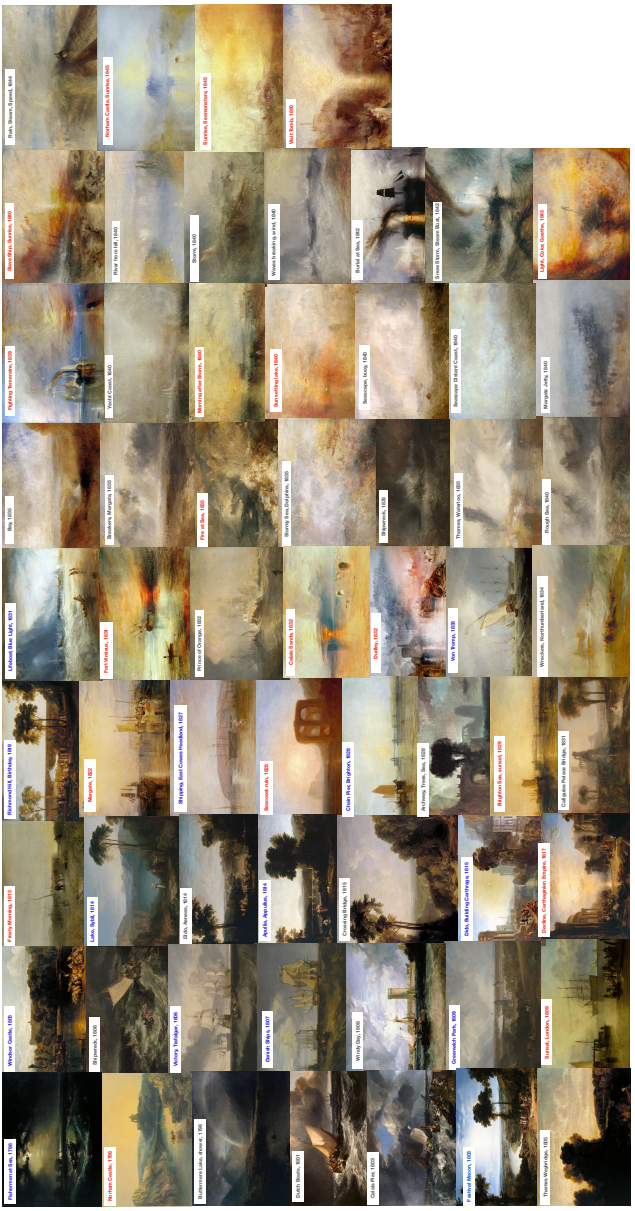

Fig. 2 60 oil paintings by Turner from 1798–1850 analyzed in Fig. 3 and Fig. 5. Each painting is indicated by keywords and year. Time goes down the columns and left to right. Text colors indicate the category: predominantly clear-sky (blue), predominantly cloudy (grey), and dawn/dusk (red). Certain paintings are cropped in this image but none are cropped in the analysis.

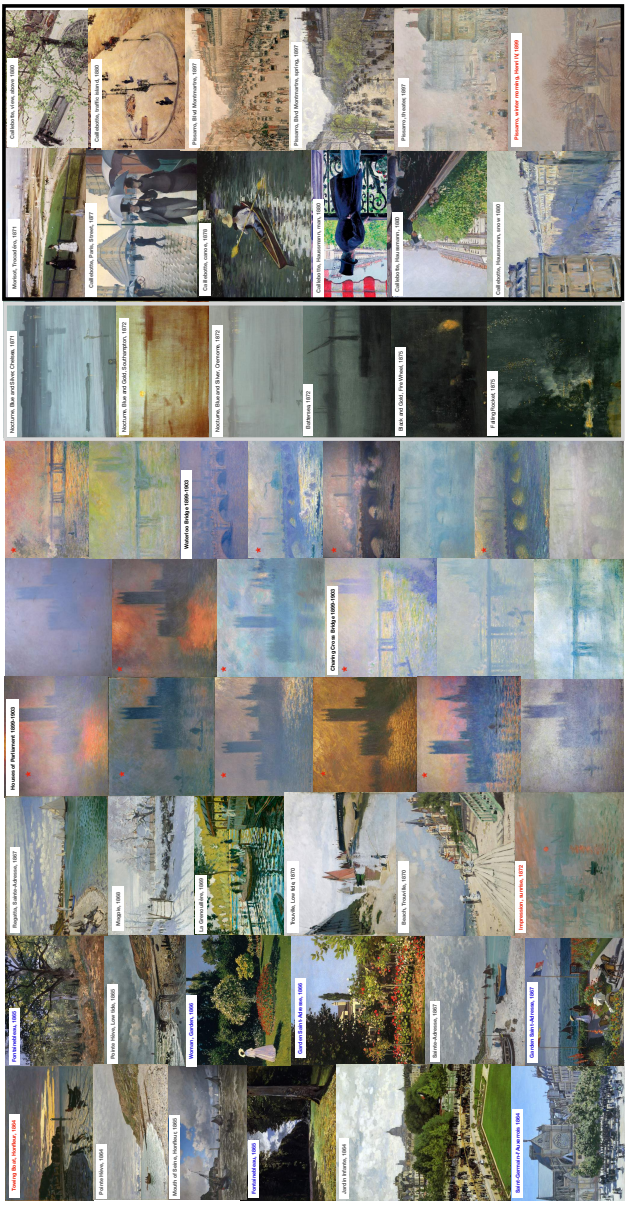

Fig. 3 38 oil paintings by Monet from 1864–1904 used in this analysis along with six from Whistler. As for Turner, we include keywords identifying the painting and its year of creation. Time goes down the columns and left to right; and colors of these keywords and date indicate the category: predominantly clear-sky (blue), predominantly cloudy (grey), and dawn/dusk (red). For Monet's series paintings in London of dawn/dusk are indicated by a red star in the top left corner. The remaining paintings are classified as predominantly cloudy or hazy. Outlined in the grey box are six London *Nocturnes* by Whistler from 1871–1875. Outlined in black are seven paintings by Caillebotte, four by Pissarro, and one by Morisot.

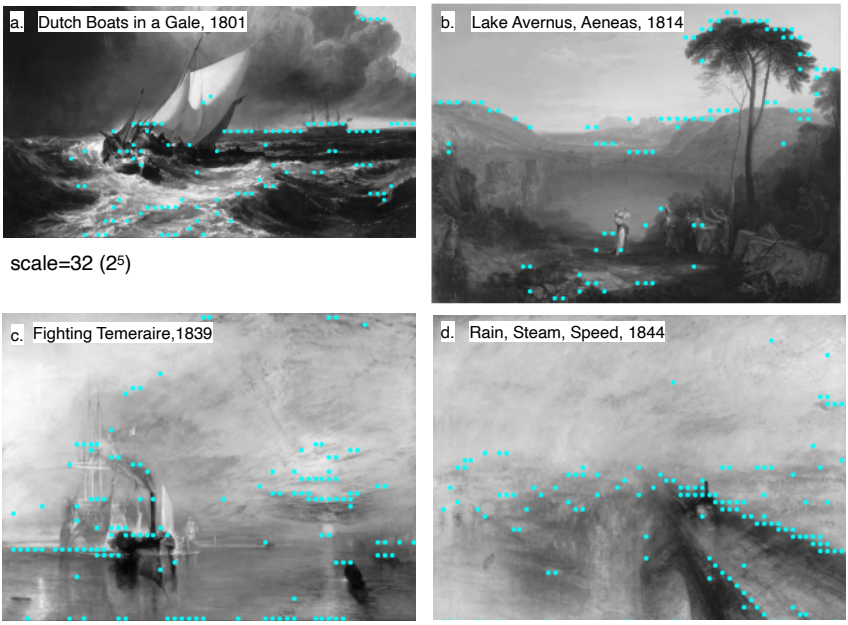

Fig. 4 Four example paintings from Turner from (a.) *Dutch Boats in a Gale* (1801); (b.) *Lake Avernus–Aeneas and the Cumaean Sybil* (1814); (c.) *The Fighting Temeraire* (1839); and (d.) *Rain, Steam, Speed* (1844). Horizontal coefficients at the fifth wavelet scale (i.e., the difference across $2^5 = 32$ pixels) that exceed the 95^{th}-percentile are indicated in each painting with cyan dots.

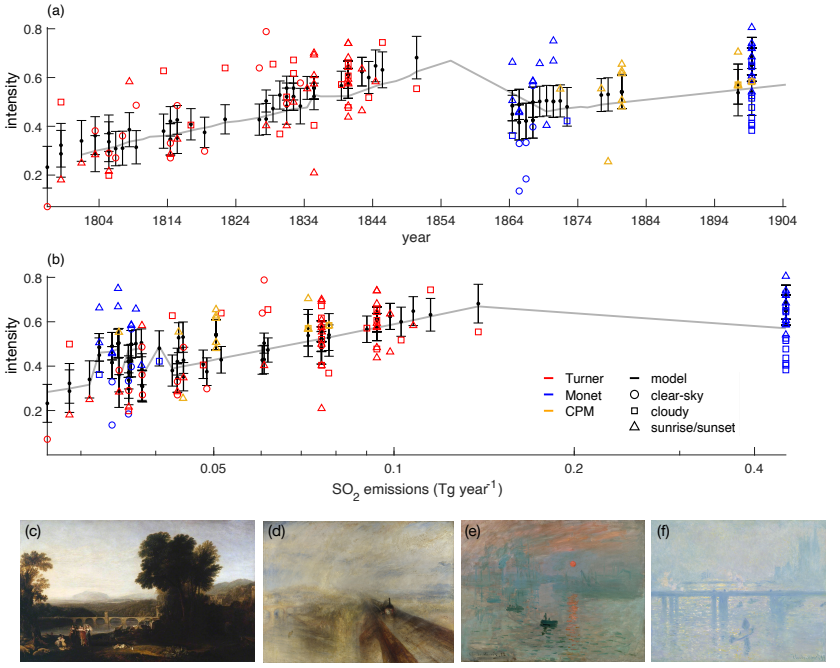

Fig. 5 Trends in the intensity index for different subjects in the 60 Turner paintings (red) and 38 Monet paintings (blue) versus (a.) year or (b.) respective London or Paris SO_2 emissions. Paintings by Caillebotte (7), Pissarro (4), and Morisot (1) are in gold. Marker styles correspond to painting type: predominantly clear-sky (circle), predominantly cloudy (square), and dawn/dusk (triangle). Black horizontal lines are model predictions, and black vertical bars indicate the 5–95% uncertainty on the model prediction. Note that year is normalized by its mean in the analysis but plotted without this normalization for reference; SO_2 is plotted on a logarithmic scale; and all Monet paintings are plotted using 1899 London emissions because paintings were begun in the winter of 1899–1900 but first exhibited in the following years, up until 1904.

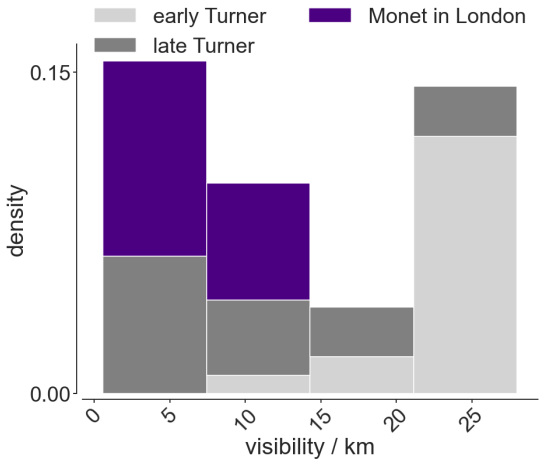

Fig. 6 Estimates of visibility using Eq. 6 for clear-sky and cloudy Turner paintings before 1830 (light grey) and after 1830 (dark grey), as well as daytime (excluding sunrise and sunset) Monet paintings in London (purple).

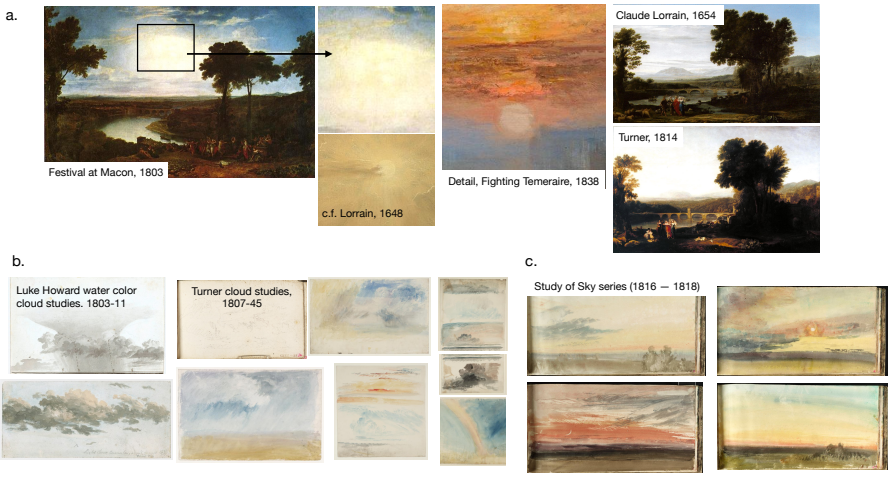

Fig. 7 Tracing Turner's awareness of growing scientific understanding of the changeability of the sun and the environment with three vignettes. Panel a. examines how Turner paints the sun and sunlight in a more dynamic, realistic way than his predecessors. Turner's *Apullia in search of Appullus* (right, lower panel) is compositionally nearly-identical to Claude Lorrain's 1654 *Landscape with Jacob and Laban and Laban's Daughters* (right, upper panel) but includes a more subtle investigation of light and darkness. Panel b. shows a subset of Turner's cloud sketches possibly influenced by Luke Howard's cloud classification. Panel c. highlights four watercolors in Turner's 'Study of Sky' series following the 1815 Tambora volcanic eruption.

Fig. 8 Various illustrations of the optical effects associated with historical London air pollution. (a): 'London. Embankment' (1908) by British photographer Frederick Evans (1853–1943). Note that photographic emulsions used prior to about the 1920s were mostly sensitive to blue light and could not differentiate clouds from non-cloudy sky, which could perhaps emphasize the hazy, luminous impression of the photograph. Atmospheric effects can therefore not be directly inferred from the image. (b) and (d) Extracts from a documentary 'Monet in the garden of Clemenceau' on *Arte* by François Prodromidès depicting London smogs, though they are taken in the early 20$^{\text{th}}$ century instead of during our period of study. (c) A sketch in the Illustrated London News, Volume 10 from the year 1847, illustrating how pedestrians and carriages were guided with torches, as the thick fogs reduced visibility even across a street, and fogs could be a cover for thievery (see lower right corner). Londoners were, moreover, aware of the dangers of fogs for health, such as increased deaths from bronchitis and other respiratory diseases, as documented in contemporary sources (as reviewed, for instance, by Corton, 2015).

References

[1] Horvath, H.: On the applicability of the Koschmieder visibility formula. Atmospheric Environment (1967) **5**(3), 177–184 (1971)

[2] Koschmieder, H.: Theorie der horizontalen sichtweite. Beitrage zur Physik der freien Atmosphare, 33–53 (1924)

[3] Gordon, J.I.: Daytime visibility, a conceptual review (1979)

[4] Jarraud, M.: Guide to meteorological instruments and methods of observation (WMO-No. 8). World Meteorological Organisation: Geneva, Switzerland **29** (2008)

[5] Vidovszky-Németh, A., Schanda, J.: White light brightness–luminance relationship. Lighting Research & Technology **44**(1), 55–68 (2012)

[6] Kim, K.W., Kim, Y.J.: Perceived visibility measurement using the hsi color difference method. Journal of the Korean Physical Society **46**(5), 1243 (2005)

[7] Singh, A., Bloss, W.J., Pope, F.D.: 60 years of uk visibility measurements: impact of meteorology and atmospheric pollutants on visibility. Atmospheric Chemistry and Physics **17**(3), 2085–2101 (2017)

[8] Singh, A., Dey, S.: Influence of aerosol composition on visibility in megacity Delhi. Atmospheric Environment **62**, 367–373 (2012)

[9] Zhao, P., Zhang, X., Xu, X., Zhao, X.: Long-term visibility trends and characteristics in the region of Beijing, Tianjin, and Hebei, China. Atmospheric Research **101**(3), 711–718 (2011)

[10] Zhang, Q., Quan, J., Tie, X., Li, X., Liu, Q., Gao, Y., Zhao, D.: Effects of meteorology and secondary particle formation on visibility during heavy haze events in Beijing, China. Science of the Total Environment **502**, 578–584 (2015)

[11] Lee, G., Gommers, R., Waselewski, F., Wohlfahrt, K., O'Leary, A.: Pywavelets: A python package for wavelet analysis. Journal of Open Source Software **4**(36), 1237 (2019)

[12] Mistry, D., Banerjee, A.: Discrete wavelet transform using matlab. International Journal of Computer Engineering and Technology (IJCET) **4**(2), 252–259 (2013)

[13] Stroup, W.W.: Generalized linear mixed models: modern concepts, methods and applications. CRC press (2012)